Nuclear Materials and Energy 17 (2018) 40–47

Contents lists available at ScienceDirect

Nuclear Materials and Energy

journal homepage: www.elsevier.com/locate/nme

Micro-structural effects of irradiation temperature and helium content in neutron irradiated B-alloyed Eurofer97-1 steel

R. Coppola[a,*], M. Klimenkov[b], A. Möslang[b], R. Lindau[b], M. Rieth[b], M. Valli[c]

[a] ENEA-Casaccia, FSN-SICNUC, Via Anguillarese 301, Roma 00123, Italy
[b] KIT-IAM, PO Box 3640, Karlsruhe D-76021, Germany
[c] ENEA-Faenza, SSTP-PROMAS-TEMAF, Via Ravegnana 186, Faenza (RA) 48018, Italy

ARTICLE INFO

Keywords:
Helium effects
Neutron irradiation
Small angle neutron scattering
Electron microscopy

ABSTRACT

The micro-structural effects of different neutron irradiation temperatures and helium contents, for 16 dpa dose, have been investigated by means of small-angle neutron scattering (SANS) in B-alloyed ferritic/martensitic steel Eurofer97-1 (0.12 C, 9 Cr, 0.2 V, 1.08 W wt%, B concentrations up to 1000 ppm); due to B transmutations, fusion relevant He/dpa values are expected to be produced under neutron irradiation. SANS measurements have been carried out on a sample irradiated at 350 °C, with estimated helium content of 5600 appm, and compared to previous SANS results, obtained on two other irradiated samples of this same B-alloyed steel. These new measurements confirm that for such high helium contents the SANS cross-section increases in order of magnitude and the magnetic SANS component is strongly reduced, compared to lower helium content (400 appm). Such effects are attributed to increase in helium bubbles density and to the presence of micro-cavities, produced after dissolution of large B-carbides. The SANS data analysis procedure has been improved, also thanks to the additional information provided by the new measurements, and more accurate helium bubble size distributions have been obtained for all the investigated samples. For 5600 appm helium content, bubble volume fractions are found of 0.025 for the sample irradiated at 350 °C and of 0.041 for the previously investigated sample irradiated at 400 °C, significantly increasing with the irradiation temperature. These values are approximately one order of magnitude larger than the value of 0.003 previously found for the sample with 400 appm helium. The size distributions are compared with electron microscopy observations of these same samples. It appears that the occurrence of complex micro-structural changes in irradiated Eurofer97-1 steel should be taken in due account when considering its application under high He/dpa ratio values.

1. Introduction

Within the frame of the "SPICE" European irradiation programme [1], the standard composition of the well-known ferritic/martensitic steel Eurofer97-1 has been modified introducing natural B contents variable between 10 ppm and 1000 ppm: in this way, under fission neutron irradiation fusion relevant helium contents and He/dpa ratios are expected to be produced by B activation. Such B-alloyed Eurofer97-1 heats have been neutron irradiated at the High Flux Reactor of the JRC-Petten, to a dose level of 16 dpa (displacement per atom) at temperatures of 250 °C, 300 °C, 350 °C and 450 °C. Reference is made to [1–7] for results of post-irradiation mechanical testing and observations by transmission electron microscopy (TEM). Results obtained on some of these sample by means of small-angle neutron scattering (SANS) are presented in Refs. [8–12]. More specifically, the results presented in Ref. [10] have shown that an Eurofer97-1 sample, with estimated helium content of 5600 appm after irradiation at 400 °C, exhibits a SANS cross section more than one order of magnitude larger compared to a sample of the same steel, irradiated at 450 °C, with estimated helium content of 400 appm helium. Moreover, for that sample containing 5600 appm helium, a strong reduction of the magnetic SANS component is observed. These SANS effects have been tentatively attributed to complex micro-structural modifications in the investigated steel. Namely, it has been suggested that for 5600 helium content the bubble distribution increases both in size and volume fraction; furthermore, the observed reduction in neutron magnetic scattering length density of the Eurofer97-1 matrix has been associated to the presence of micro-cavities as large as 10 μm, originated by the dissolution of B-carbides due to transmutation under irradiation [10].

* Corresponding author.
E-mail address: roberto.coppola@enea.it (R. Coppola).

https://doi.org/10.1016/j.nme.2018.08.005
Received 10 May 2018; Received in revised form 4 July 2018; Accepted 17 August 2018

In order to confirm and further investigate the origin of this simultaneous increase in SANS cross-section and decrease in magnetic SANS component, new SANS measurements have been carried out on another Eurofer97-1 sample containing 5600 appm helium and irradiated at 350 °C. These new SANS results have provided additional experimental information, useful also to improve the previously adopted SANS data analysis procedure. In this way, the uncertainties associated to the fitting have been reduced and more accurate size distributions have been obtained for all the investigated irradiation conditions, namely: three different irradiation temperatures and two helium contents, for same dose level of 16 dpa. As discussed in the previous papers [10,11] and here below (Section 3), the micro-structural effects of neutron irradiation in such B-alloyed are very complex: in fact, in addition to the effects relating to the dissolution of large B-carbides, a simultaneous occurrence of micro-voids and helium bubbles is to be expected, hardly distinguishable from each other both by SANS and by TEM. Therefore, the suggested interpretation of the SANS results and related analysis is not intended as a conclusive one, but as a new contribution to progress in understanding the micro-structural radiation damage effects in Eurofer97-1 under conditions close to those expected in a fusion reactor.

2. Material characterization

The standard chemical composition of Eurofer97-1 is the following: 0.12 C, 9 Cr, 0.2 V, 1.08 W Fe bal wt%. It has been modified introducing, by mechanical alloying, ^{10}B contents of 0.0083 mass-% ("ADS3" heat) and of 0.1120 mass-% ("ADS4" heat): under neutron irradiation, they correspond to estimated helium concentrations of 400 appm and 5600 appm respectively. The irradiated samples prepared for the SANS measurements were platelets, approximately 4 × 9 mm^2 in surface and 1 mm thick; they were cut from the KLST specimens prepared for post-irradiation mechanical testing [1]. The reference, un-irradiated samples were approximately 1 cm^2 in surface and 1 mm thick; they had been submitted to the standard treatment 1040 °C 30′ + 760 °C 1.5 h, like the irradiated ones. The micro-structural effect of ageing at 450 °C, for a duration equivalent to the irradiation time (770 days) has been checked experimentally, finding no differences between the SANS cross-sections of the un-aged and aged sample [12].

TEM observations of these irradiated samples [3,6] show various morphological changes, particularly in the samples containing 5600 appm helium. In fact, under neutron irradiation the dissolution of B precipitates (BN, $M_{23}(C,B)_6$) leaves empty regions or micro-cavities as large as a few μm. Around such cavities subsequent halos are formed with high concentrations of helium bubbles or micro-voids, often characterized by bi-modal size distributions [3]. This effect, theoretically investigated for the more general case of transmutation-induced deposition profiles in steels [13], is shown in Fig. 1 referring to an Eurofer97-1 sample with 5600 appm helium after irradiation at 300 °C–16 dpa [14]. As discussed in Refs. [3,6], the TEM observed bubble distributions appear much more influenced by the ^{10}B content, therefore by the helium content, than by the irradiation temperature. It is noted that the TEM resolution power decreases strongly for sizes below 10 Å and that it is not easy to distinguish by this technique helium bubbles from micro-voids. The size histograms presented in Ref. [6] are compared with the SANS size distributions in Section 3 here below.

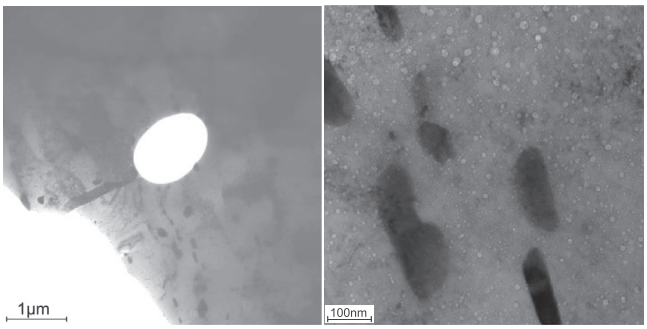

Fig. 1. Eurofer97-1 sample, containing 5600 appm helium after irradiation at 300 °C to 16 dpa; formation of halos containing bubbles/cavities around the hole [14].

3. Experimental technique and data analysis

The application of the SANS technique to the case of a magnetic steel has been presented in the previous works on this subject [8–12]; more general information on SANS can be found in Refs. [15,16]. The measurements have to be carried out applying to the investigated sample an external magnetic field of at least 1 T in order to saturate its magnetization. In this way, it is possible to measure separately the nuclear and magnetic components of the SANS cross-section, defined as follows:

$$d\Sigma(Q)/d\Omega = d\Sigma(Q)/d\Omega_{nucl} + d\Sigma(Q)/d\Omega_{mag}\sin^2\alpha, \quad (1)$$

where 2θ is the full scattering angle, λ the neutron wavelength, $Q = 4\pi sin\theta/\lambda$ the modulus of the scattering vector, α the azimutal angle on the detector plane and Ω stands for the solid angle. The ratio of the SANS components measured in the directions perpendicular and parallel to the magnetic field is defined as follows:

$$R(Q) = \frac{d\Sigma(Q)/d\Omega_{nucl} + d\Sigma(Q)/d\Omega_{mag}}{d\Sigma(Q)/d\Omega_{nucl}} = 1 + (\Delta\rho)^2_{mag}/(\Delta\rho)^2_{nucl} \quad (2)$$

it is related to the nuclear and magnetic square differences in neutron scattering length density between the defects and the matrix,$(\Delta\rho)^2_{nucl}$ and $(\Delta\rho)^2_{mag}$ respectively [15,16]; its dependence on Q implies that defects of different composition contribute in the measured total SANS cross-section. In Eurofer97-1, assuming for the carbides a composition $Cr_{14}Fe_8W_{0.7}V_{0.3}C_6$ [17] a nuclear contrast value of 2.13 10^{20} cm^{-4} is found for such precipitates; for micro-voids, the contrast is equal to the scattering length density of Eurofer97-1 itself, that is 5.51 10^{21} cm^{-4}, while for helium bubbles it is 4.88 10^{21} cm^{-4} [16]. Therefore, for comparable values of the corresponding volume fractions, both helium bubbles and micro-voids are expected to give rise to SANS effects one order of magnitude larger than precipitates, but on the other hand are quite difficult to be distinguished from one another.

The distributions of the scattering defects are obtained by inverse transformation of the experimental data. Namely, if their volume fraction is low and there is no inter-particle interference (dilute system), the SANS nuclear and magnetic cross-sections can each one be written as

$$d\Sigma(Q)/d\Omega = (\Delta\rho)^2 \int_0^\infty dR\, N(R)\, V^2(R)\, |F(Q,R)|^2 \quad (3)$$

where $N(R)$ is the number per unit volume of defects with a size between R and $R + dR$, V their volume, $|F(Q,R)|^2$ their form factor (assumed spherical in this case) and $(\Delta\rho)^2$ is the nuclear or magnetic "contrast".

The volume distribution function $D(R)$, average defect radius, $\langle R\rangle$, and volume fraction, f, are defined respectively as follows:

$$D(R) = N(R)R^3 \quad (5)$$

$$< R > = \int_0^\infty dR\, N(R)R/.\int_0^\infty dR\, N(R) \quad (6)$$

$$f = \int_0^\infty dR\, N(R)V(R)/.(\Delta\rho^2)\, V_{tot} \quad (7)$$

where V_{tot} is the total volume of the investigated sample.

$N(R)$ was determined by the mathematical method described in Ref. [18] and successfully utilized for several studies on technical steels, particularly those in Refs. [19,20]. This fitting procedure assumes no *a-*

priori shape for the size distribution, but represents it by a set of cubic B-spline functions, with knots uniformly distributed in a log R scale and with the constraint $N(R) > 0$. Such logarithmic scale is quite suited for poly-disperse distributions, in the presence of defects with sizes differing in order of magnitude. The number of splines is determined by the R-range where the size distribution is to be investigated, $R_{min.} - R_{max.}$, and by the required degree of detail; an excessive number of such splines can introduce unphysical oscillations in the obtained distribution. Knots spacing, R-range and a constant or Q-dependent background are additional parameters, adjustable for improving the fit. The best-fit distribution is determined within an 80% confidence band, which reflects on the reliability of the obtained metallurgical information, namely defect average size and volume fraction. The inverse transformation of Eq. (3) is in itself a relatively simple mathematical problem. Difficulties arise from the fact that the SANS cross-section is measured only on a finite Q-interval, in a limited number of points (with experimental errors) and without the reference of a theoretical model distribution, usually not available for such technical steels. All this must be taken into account in selecting the fitting parameters, in order to obtain plausible distributions and, at the same time, reduce their error band as much as possible.

4. Results

The SANS measurements were carried out at the D22 instrument at the High Flux Reactor of the Institut Max von Laue - Paul Langevin (ILL), Grenoble. Due to safety regulations, the irradiated samples had to be transported to the neutron source in different times and included in separate SANS experiments: in fact their activity level was 4.42 10^{10} Bq, with contact dose rate in an Al capsule of 14 mSv/h. The same reference, un-irradiated Eurofer97-1 sample ("ADS3" heat) was included in each experiment for a check. The Eurofer97-1 sample irradiated at 350 °C, containing 5600 appm helium, and the un-irradiated reference (``ADS4" heat) were measured in the same conditions as the previously measured sample irradiated at 400 °C, containing 5600 appm helium, namely $\lambda = 6$ Å and sample-to-detector distances of 3.5 m and 11.2 m (Q interval ranging from 2 10^{-3} Å^{-1} to 0.16 Å^{-1}, particle sizes $2R \sim \pi/Q$ ranging from 20 Å to 1500 Å approximately). Additionally, these two samples were shortly tested at $\lambda = 11.5$ Å and sample-to-detector distance of 17.6 m, but without calibration to absolute scale. The sample containing 400 appm helium and its un-irradiated reference had been measured with $\lambda = 6$ Å and sample-to-detector distances of 2 m and 11.2 m, over a Q-interval ranging from 3 10^{-3} Å^{-1} to 2.6 10^{-1} Å^{-1} (sizes varying between 10 Å and 1000 Å approximately). All these measurements were carried out under an external 1 T magnetic field. For calibration to absolute SANS cross-section value in physical units the ILL standard programs [21] were utilized, obtaining statistically evaluated experimental errors generally below 3%. The nuclear and nuclear plus magnetic SANS cross-sections were determined by selecting on the 2D detector plane sectors 15° wide around the directions parallel and perpendicular to the external magnetic field respectively.

Fig. 2a–c show, for $\lambda = 6$ Å and sample-to-detector distance of 11.2 m, the 2D SANS pattern of the sample irradiated at 350°, containing 5600 appm helium, together with the previously measured ones [8,10]: compared to the sample with 400 appm helium, it appears nearly isotropic with respect to the external magnetic field, but not as much isotropic as the other sample with 5600 appm, irradiated at 400 °C. Fig. 3a and b show, for $\lambda = 11.5$ Å and sample-to-detector distance of 17.6 m, the 2D SANS patterns measured for the two samples containing 5600 appm helium: in this Q-range, corresponding to defect sizes as large as 3000 Å, the sample irradiated at 350 °C exhibits the 2D pattern magnetic anisotropy typical of fully magnetized steels, while the pattern of the sample irradiated at 400 °C is isotropic. The nuclear SANS cross-section and $R(Q)$ ratio measured for the sample irradiated at 350 °C, with 5600 appm helium, are shown in Fig. 4a and b respectively, together with nuclear SANS cross-section and $R(Q)$ of reference samples and previously measured irradiated samples. There is good agreement in the SANS cross-sections of the reference samples; therefore the results obtained in the different experiments on the irradiated samples can safely be compared.

The measurement of the sample irradiated at 350 °C, with 5600 appm helium, adds significant information on neutron irradiated Eurofer97-1. First, it confirms that for very high helium content a strong increase in SANS cross-section and decrease in magnetic SANS component are observed. Furthermore, it proves very useful to progress in understanding how the micro-structure evolves under increasingly severe irradiation conditions.

In fact, for 400 appm helium and a relatively high irradiation temperature (450 °C), the effect of the irradiation on the SANS cross-section is detected only for 3 10^{-2} Å$^{-1} < Q <$ 2.6 10^{-1} Å^{-1}, corresponding to defect radii smaller than 50 Å approximately. For $Q <$ 3 10^{-2} Å^{-1}, there is no detectable difference between reference and irradiated samples; both follow a "Porod behavior" (Q^{-4} power law) [15,16], typical of very large micro-structural defects outside the available experimental window. This is attributed to the presence of carbide precipitates [17], larger than approximately 500 Å; they remain nearly un-changed during the irradiation [8,10]. A nearly constant value of $R(Q)$, close to 2, is measured (Fig. 4b), implying the presence of non-magnetic defects, such as helium bubbles or micro-voids embedded in a fully magnetized matrix (Eq. (2)). For such helium content, the measured SANS effect is quite similar to the one measured in standard Eurofer97-1 irradiated to 16 dpa at 250 °C, with no enhanced helium production [11].

For 5600 appm helium content and 350 °C irradiation temperature, an increase of one order of magnitude in the SANS cross-section is detected, compared to 400 appm helium content, for $Q >$ 2.10^{-2} Å^{-1} approximately, with a nearly isotropic 2D pattern (Fig. 2b) and $R(Q) \sim 1.3$ (Fig. 4b). For smaller Q values, the cross-section decreases then approaches the Porod behavior of the un-irradiated, reference sample; at even smaller Q values an anisotropic 2D pattern is detected with respect to magnetic field (Fig. 3a). For 5600 appm helium content and 400 °C irradiation temperature, over all the investigated Q range a strong increase in SANS cross-section and a 2D isotropic pattern, with $R(Q) \sim 1.3$, have been measured [10].

Therefore, the comparison of the SANS results obtained on these three samples suggests how the original micro-structure of the un-irradiated Eurofer97-1 (few large carbides, in a fully magnetic matrix) is modified under the simultaneous effect of fission neutron irradiation and enhanced helium production. First, a distribution of small defects appears, consisting most probably in a mixture of helium bubbles and micro-voids. When the helium content and the irradiation temperature are significantly increased, a much broader distribution of helium bubbles and apparent de-magnetization of the steel matrix progressively develop.

The size distributions have been determined taking for the neutron contrast the value corresponding to the helium bubbles (4.88 10^{21} cm^{-4}), which is very close to the contrast value for micro-voids as mentioned here above. This value has been included in the iterative transformation procedure of Eq. (3) and utilized for determining the volume fraction as defined in Eq (7). As a first approximation, the contrast dependence on the helium bubble radius has not been included in the fitting procedure, since its effect on the distributions is significant only for bubbles larger than 100 Å approximately [22,23]. The influence of the fitting parameters has been systematically checked, particularly for the sample irradiated at 400 °C with 5600 appm helium. Better results, compared to those presented in Ref. [10], have been obtained reducing the number of splines (from 7 to 4 or 5) and increasing the $R_{min.}$ to at least 3 Å, which can be considered the minimum size for observable bubbles or micro-voids. Furthermore, the measurement of the sample irradiated at 350 °C shows that also for very high helium content a strong SANS contribution from the large carbide precipitates can be present. Consequently, a number of points at low Q-

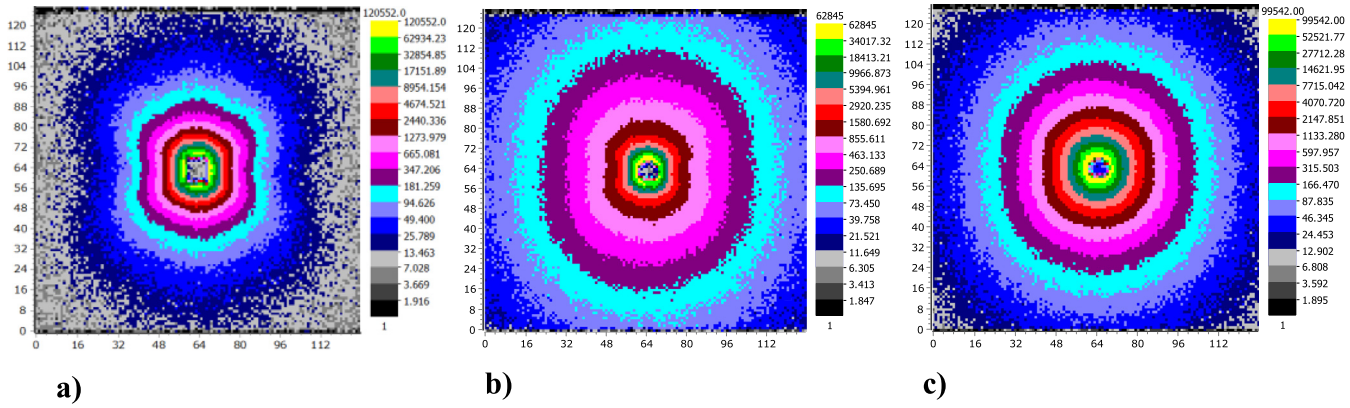

Fig. 2. 2D SANS patterns (un-calibrated neutron counts) measured with λ = 6 Å and sample-to-detector distance of 11.2 m, for Eurofer97-1 irradiated at 350 °C dpa, with 5600 appm helium (b), compared to Eurofer97-1 irradiated at 450 °C with 400 appm helium (a) and irradiated at 400 °C with 5600 appm helium (c) [8,10]. The direction of the external magnetic field is horizontal in the plane of the figure.

values has not to be considered when fitting the SANS cross-section to obtain the helium bubble distribution. Excluding such points, instead than fitting the difference between irradiated and reference sample as previously made [10], has resulted in a further improvement of the fit, since that difference introduces additional experimental errors. Both ways to proceed contain an unavoidable degree of arbitrariness: in fact, from the experimental data of Fig. 4a it is not straightforward to decide where exactly the asymptotic SANS effects of the large precipitates can be neglected. For the sample irradiated at 400 °C, containing 5600 appm helium, a good fit was obtained over all the investigated *Q*-range.

The obtained size and volume distributions, together with the corresponding fits to the experimental data, are shown in Figs. 5–7. For the sample irradiated at 450 °C, with 400 appm helium content, monodisperse size and volume distributions are found (Fig. 5a), with an average radius of 7 Å and a volume fraction of 0.003. Only the SANS cross-section measured at 2 m sample-to-detector distance has been considered, as already made in [10]; to obtain a good fit (Fig. 5b), it was necessary to exclude the experimental points apparently "contaminated" by the effect of the large carbides ($Q < 5.5\ 10^{-2}$ Å^{-1}) and the few ones at the highest *Q*-values, where the difference with the reference sample is comparable to the experimental errors. For the sample irradiated at 350 °C, with 5600 appm helium, much broader distributions are obtained (Fig. 6a), requiring the logarithmic scale to show the volume one; an average radius of 13 Å and a volume fraction of 0.025 are found. Also for this sample, the effect of the large carbides has been taken into account, excluding from the fit the points measured for $Q < 10^{-2}$ Å^{-1} (Fig. 6b). For the sample irradiated at 400 °C, with 5600 appm, even broader distributions are found (Fig. 7a) and the volume one appears markedly bi-modal. The average radius as defined in Eq. (6) is equal to 13 Å, with a secondary population radius around 90 Å; a volume fraction of 0.041 is obtained. A good fit is obtained over all the investigated *Q*-range (Fig. 7b).

For qualitatively comparing with the available TEM histograms [6] in the overlap region, the volume distributions have been considered. In fact, *N(R)* is a *differential* number of defects per unit volume, while the number of defects counted by TEM observations is not normalized to the investigated sample volume. Furthermore, the SANS cross-section is weighted with the square volume of the observed defects (Eq. (3)). This qualitative comparison is shown in Fig. 8a–c. A good agreement is found for the sample irradiated at 450 °C, with 400 appm helium (Fig. 8a), taking into account the difficulty to observe by TEM, in a

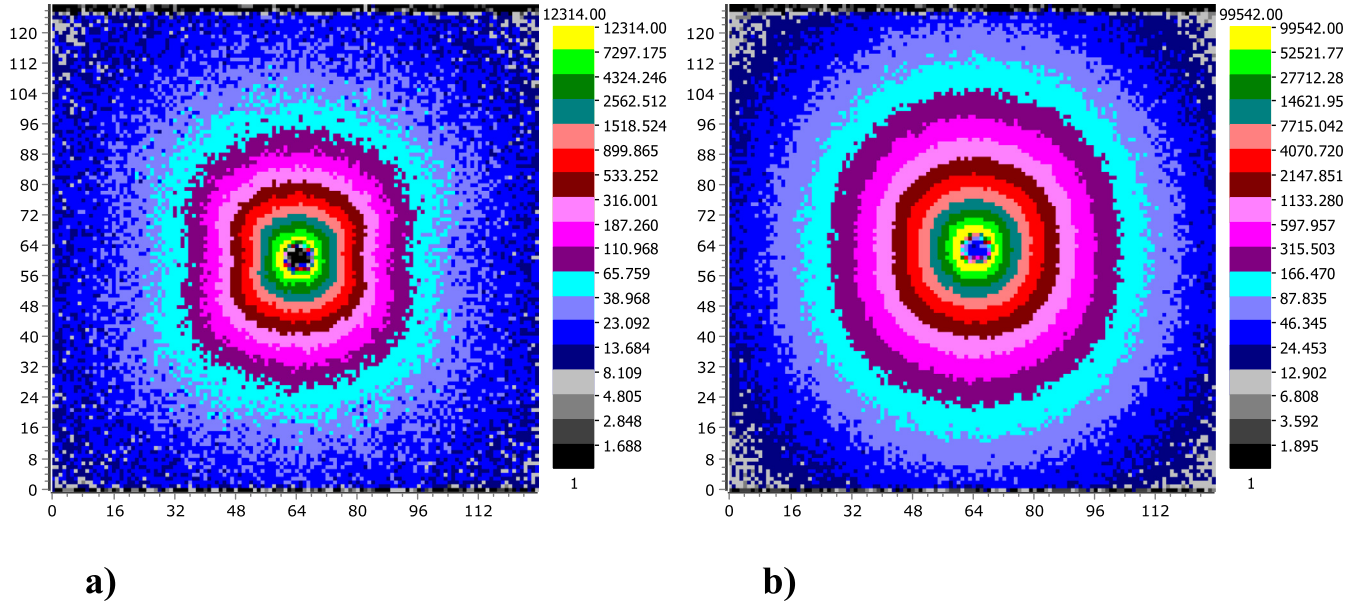

Fig. 3. 2D SANS patterns (un-calibrated neutron counts) measured with λ = 11.5 Å and sample-to-detector distance of 17.6 m, for Eurofer97-1 irradiated at 350 °C dpa, with 5600 appm helium (a), compared to Eurofer97-1 irradiated at 400 °C with 5600 appm helium (b). The direction of the external magnetic field is horizontal in the plane of the figure.

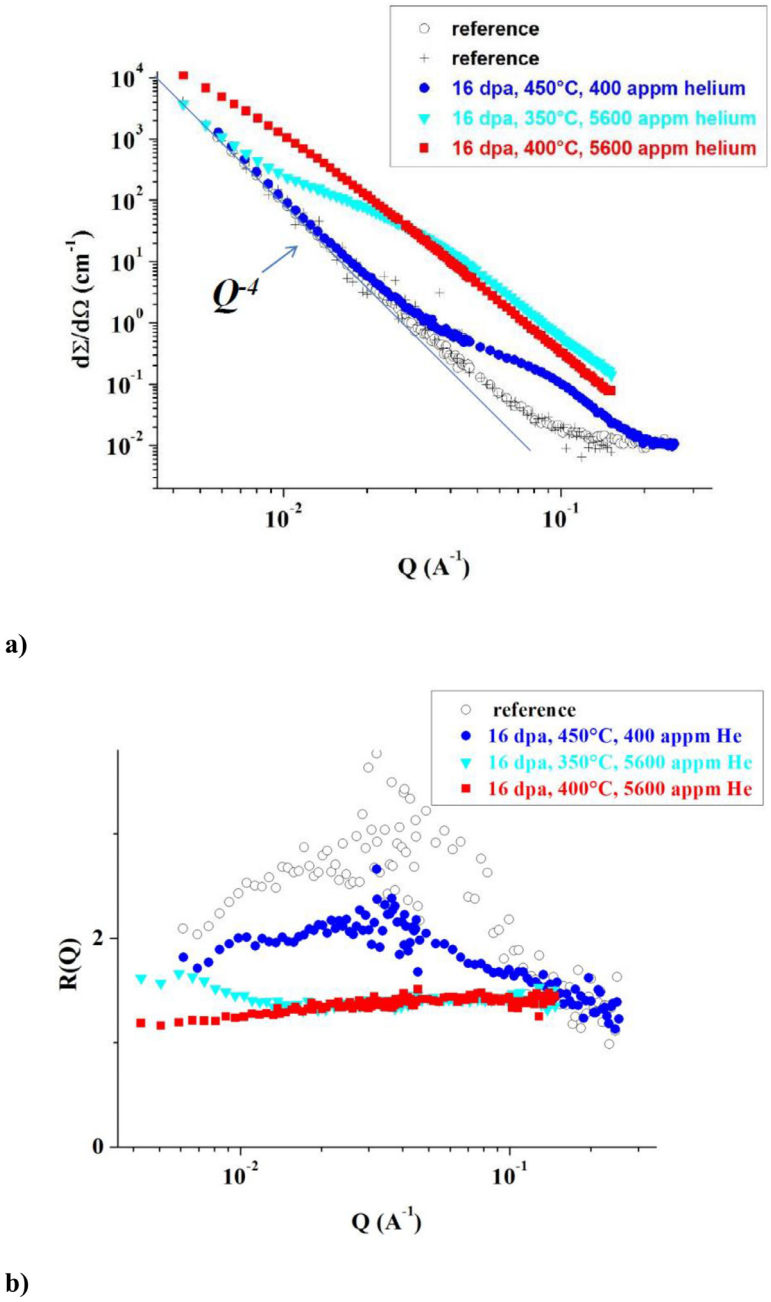

Fig 4. Nuclear SANS cross-section (a) and *R(Q)* (b) for Eurofer97-1 irradiated at 350 °C dpa, with 5600 appm helium (triangles, cyan) and for ADS4 reference (crosses), compared to previous measurements [8,10] of ADS3 reference (empty circles), Eurofer97-1 irradiated at 450 °C with 400 appm helium (full circles, blue) and Eurofer97-1 irradiated at 400 °C with 5600 appm helium (squares, red). In a), the Q^{-4} power law behavior is shown.

magnetic steel, defects smaller than 10 Å. The volume distribution obtained for the sample irradiated at 350 °C, with 5600 appm helium, is compared in Fig. 8b with the histogram determined for another sample with same helium content, but irradiated at 300 °C (not available for 350 °C). Also in this case, TEM seems to underestimate the presence of bubbles smaller than 10 Å, but additionally the SANS result gives a much broader distribution, extended up to 100 Å. This discrepancy is more severe for the sample irradiated at 400 °C with 5600 appm helium (Fig. 8c), not only for the small radii (the TEM histogram includes only values larger than 25 Å), but also for the larger ones; in the case of this sample, given the very large sizes of the bubbles such discrepancy can be explained by truncation effects, due to poor statistics and to the difficulty of thinning the sample without destroying the larger bubbles. Average radii and volume fractions, attributed to the helium bubbles, are summarized in Table 1. The errors resulting from the obtained 80% confidence bands (Figs. 5–7) are a few %. However, it must be considered that such distributions are obtained under the assumptions described here above, necessary to attempt an interpretation of the obtained SANS results in the absence of a theoretical model to compare with. An estimate of the uncertainties resulting from different methodological assumptions and choice of the fitting parameters is provided by the comparison with the distributions presented in Ref. [10], for the two previously investigated samples. For instance, for the sample irradiated at 450 °C, with 400 appm helium, a volume fraction of 0.007 had been obtained setting $R_{min.} = 1$ Å and including in the fit also the few points at the highest *Q* values: in this way, spurious contributions both from the background noise and from the large carbides were probably not completely suppressed. For the sample irradiated at 400 °C, with 5600 appm helium, a volume fraction of 0.038 had been determined, in agreement with the new one, but the new distribution (Fig. 7a) is

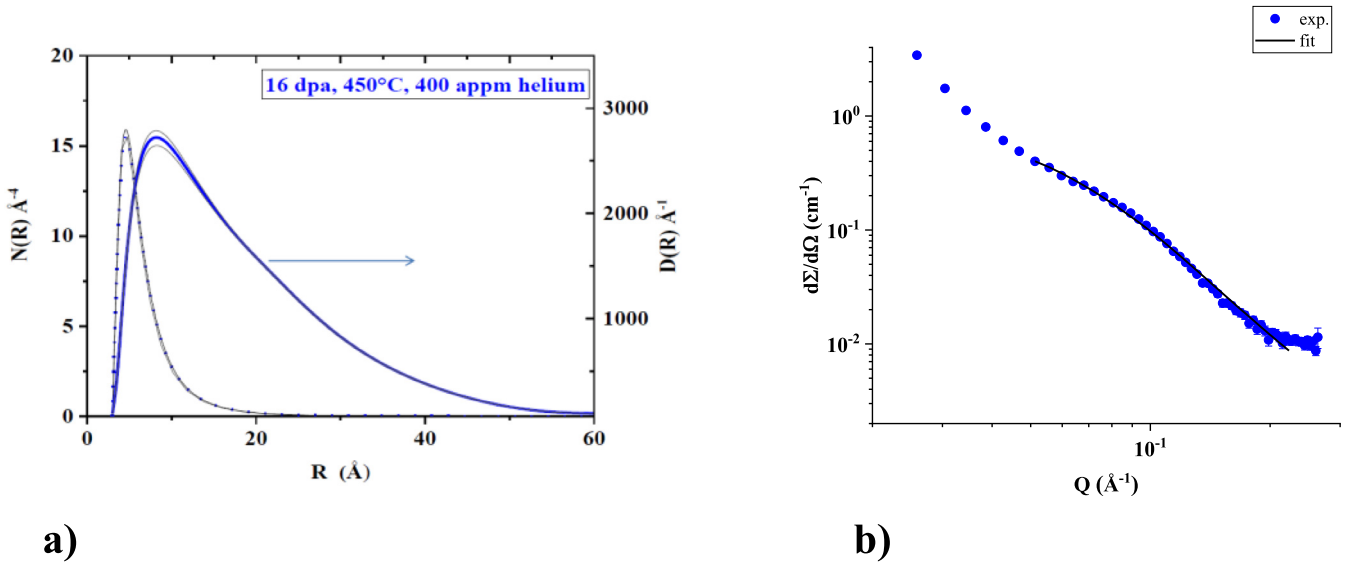

Fig. 5. Eurofer97-1 irradiated at 450 °C with 400 appm helium: (a) size (left scale, dots) and volume (right scale, continuous line) distributions attributed to the helium bubbles, the black lines represent the extremes of the 80% confidence band; (b) fit to the experimentally measured nuclear SANS cross-section.

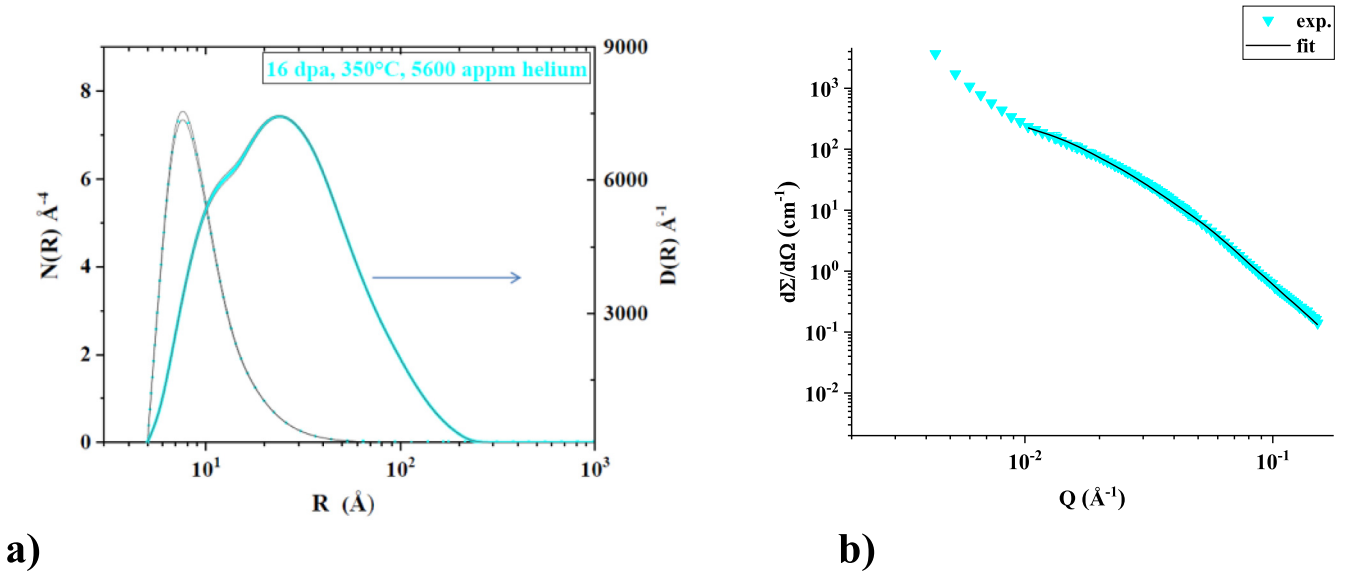

Fig. 6. Eurofer97-1 irradiated at 350 °C with 5600 appm helium: (a) size (left scale, dots) and volume (right scale, continuous line) distributions attributed to the helium bubbles, the black lines represent the extremes of the 80% confidence band; (b) fit to the experimentally measured nuclear SANS cross-section.

determined with higher resolution and much smaller error band. In Table 1, the volume fractions are compared with the two available TEM determined swelling values [6], defined as total apparent bubble volume divided by total observation volume. There is agreement for the sample irradiated at 450 °C with 400 appm helium, while for the sample irradiated at 400 °C, with 5600 appm helium, the volume fraction is one order of magnitude larger; this is consistent with the qualitative comparisons shown in Fig 8a and c.

5. Discussion and conclusions

The new SANS measurements presented in this paper confirm the previously observed neutron irradiation effects in B-alloyed Eurofer97-1 with high helium content. Furthermore, improvements in the SANS data analysis lead to better understanding the micro-structural evolution of this steel. It could certainly be remarked that investigating by SANS a larger number of such irradiated samples would be necessary; however, investigating just three of them has already implied a remarkable effort both for SANS measurements and TEM observation, for handling and transportation to the neutron source. The current knowledge of the investigated metallurgical problem allows only a tentative interpretation, but the observed SANS effects are marked and clear, so these results allow some conclusions on the micro-structural effect of increasingly severe irradiation conditions in Eurofer97-1.

The observed increases in the SANS cross-sections (Fig. 4a) are attributed to the development of micro-voids and helium bubbles distributions; this assumption is based on their higher “visibility” by this technique, compared to precipitates (Section 3). Furthermore, TEM observations show that such defects appear the dominant ones. For 400 appm helium content, the already mentioned comparison with the SANS cross-section of neutron irradiated standard Eurofer97-1 [11] suggests that a mixture of micro-voids and bubbles is present. Furthermore, the SANS cross-section of an Eurofer97-1 sample, irradiated at 450 °C with 80 appm helium [12], is only slightly smaller than the one measured for the sample with 400 appm helium (Fig. 4a), with a volume fraction of 0.002. This suggests that up to 400 appm the effect

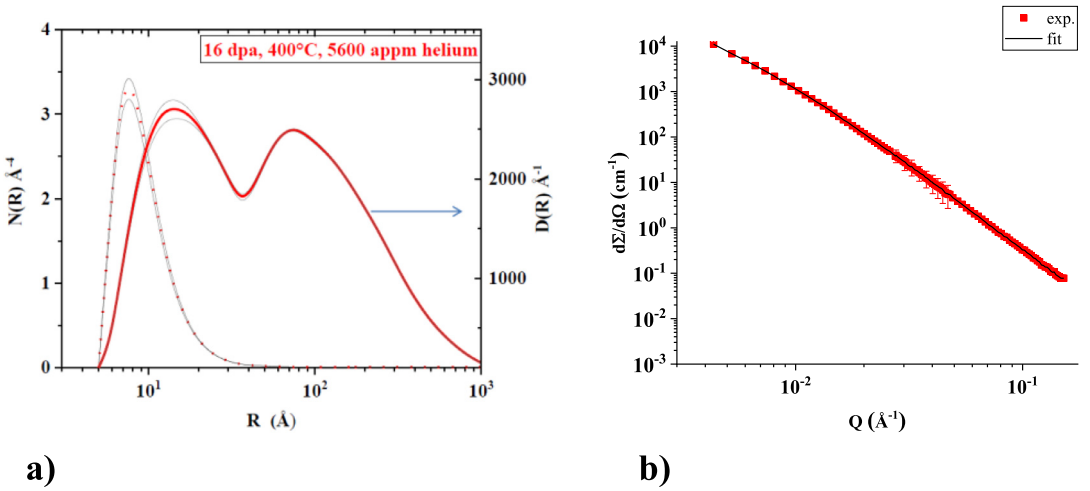

Fig. 7. Eurofer97-1 irradiated at 400 °C with 5600 appm helium: (a) size (left scale, dots) and volume (right scale, continuous line) distributions attributed to the helium bubbles, the black lines represent the extremes of the 80% confidence band; (b) fit to the experimentally measured nuclear SANS cross-section.

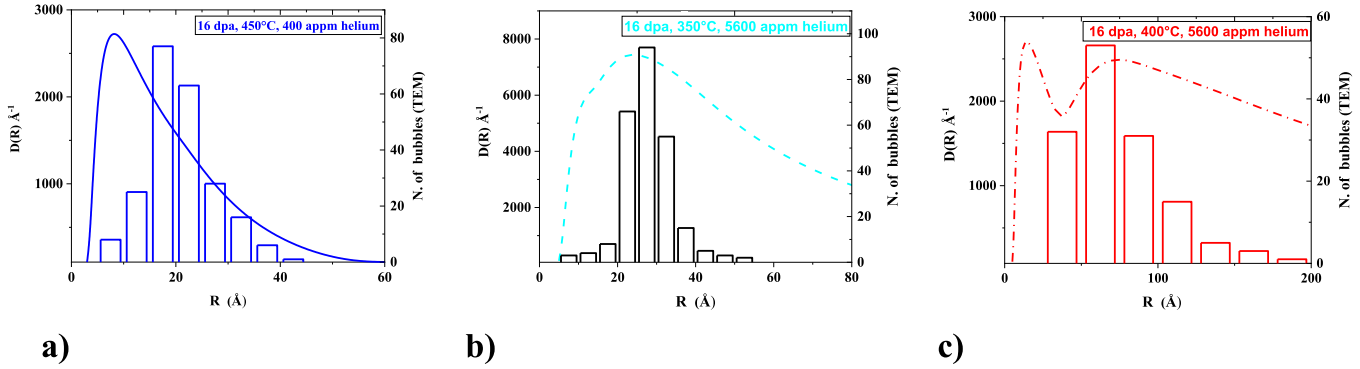

Fig. 8. SANS obtained distributions (left scales) for Eurofer97-1 (a) irradiated at 450 °C 400 appm helium, (b) irradiated at 350 °C 5600 appm helium, (c) irradiated at 400 °C 5600 appm helium, compared to corresponding TEM histograms [6] (right scales). The TEM histogram in (b) refers to Eurofer97-1 irradiated at 300 °C, 5600 appm helium. Both the SANS distributions and the TEM histograms are attributed to helium bubbles.

of the helium concentration is significantly smaller compared to the dpa one. For 5600 appm helium, at both the investigated irradiation temperatures the strong increase in SANS cross-sections is attributed mostly to helium bubbles. Concerning more specifically the sample irradiated at 400 °C with 5600 appm helium, the bi-modal distribution in Fig. 7a fits very well the shape of the corresponding cross-section. In this Q-range, the large micro-cavities should contribute with a Q^{-4} power law, which is not observed at all; therefore, it seems appropriate to attribute the observed SANS effect to two different populations of helium bubbles. They are indeed observed in large density by TEM in such samples (Fig. 1 and Refs. [6,7]), but apparently it is not easy to quantitatively convert such observations into high statistics histograms. In this regard, reference is made to [24] for a discussion of truncation effects in TEM observation of very large defects. The two samples containing 5600 appm helium could not be investigated at sufficiently high Q to compare their incoherent scattering with the one of the un-irradiated, reference sample (Fig. 4a); this will be necessary to more accurately evaluate the contribution from the helium bubbles as small as a few Å.

Table 1
– Volume fractions, f, and average radii, $\langle R \rangle$, attributed to the helium bubbles, for the investigated Eurofer97-1 samples, compared with the available swelling values determined by TEM [6].

Irradiated sample (16 dpa)	*f (TEM swelling [6])*	$\langle R \rangle$
450 °C, 400 appm helium	0.003 (0,0015)	7 Å
350 °C, 5600 appm helium	0.025	13 Å
400 °C, 5600 appm helium	0.041 (0,0042)	13 Å (secondary 90 Å)

The measurement of the sample irradiated at 350 °C provides an essential confirmation of the previously observed reduction in magnetic SANS component. In fact, in the two samples containing 5600 appm helium this effect appears correlated with the severe damage produced under irradiation for such correspondingly high alloyed B-contents and B-carbides distributions (Fig. 1). The nearly isotropic SANS patterns shown in Figs. 2b and c and 3 imply a very small, or null magnetic contrast (Eq (2)), with scattering defects embedded in a no longer fully magnetized matrix. The effect of this apparent de-magnetization of the Eurofer97-1 matrix appears sensitive to a 50 °C increase in the irradiation temperature, as particularly evident in Fig. 3. That suggests that not only the helium content, but also the irradiation temperature plays a relevant role in the degradation of B-alloyed Eurofer97-1. SANS measurements with higher magnetic field and polarized neutron beam are also planned to further investigate this aspect. The experimental data obtained on the samples with 5600 appm helium should also be completed by SANS measurements extended not only in the high Q region, for evaluating the background, but also in the low Q one, with calibration to absolute scale to quantitatively compare their nuclear and magnetic cross-sections.

As a final remark, it should be emphasized that fission neutron irradiation of B-alloyed Eurofer97-1 *simulates* the damage and He/dpa ratio expected by 14 MeV neutrons in a tokamak and probably overestimates this ratio with respect to the real working conditions. This point is discussed in the review paper of Ref. [25], where the results of several irradiation experiments on Eurofer97-1 are analyzed. Anyhow,

the obtained SANS results, referred to macroscopic sample volumes, complete the information obtained on these same samples by TEM and suggest that a severe micro-structural degradation of the Eurofer97-1 should be taken in due account for high helium contents.

Declaration of interests

The authors declare that they have no known competing financial interests or personal relationships that could have appeared to influence the work reported in this paper.

Acknowledgments

This work has been carried out within the frame of the EUROfusion Consortium and has received funding from the Euratom research and training programme 2014–2018 under grant agreement No 633053. The views and opinions expressed herein do not necessarily reflect those of the European Commission.

References

[1] E. Materna-Morris, A. Möslang, S. Baumgärtner, J. Ehrmann, E. Gaganidze, M. Holzer, S. Lautensack, H. Ries, R. Rolli, H.-C- Schneider, H. Zimmermann, FZK Rep. IMF I No. 092 FUSION N0323, December 2008.
[2] E. Materna-Morris, A. Möslang, R. Rolli, H.-C. Schneider, J. Nuc. Mat. 386-388 (2009) 422–425.
[3] M. Klimenkov, A. Möslang, E. Materna-Morris, H.-C. Schneider, J. Nuc. Mat. 442 (2013) S52–S57.
[4] M. Klimenkov, A. Möslang, E. Materna-Morris, Micron 46 (2013) 51–56.
[5] E. Materna-Morris, M. Klimenkov, A. Möslang, Mat. Sc. For. 730-732 (2013) 877–882.
[6] M. Klimenkov, A. Möslang, E. Materna-Morris, J. Nuc. Mat. 453 (2014) 54–59.
[7] M. Klimenkov, E- Materna-Morris, A. Möslang, J. Nucl. Mat. 462 (2015) 280–288.
[8] R. Coppola, M. Klimenkov, R. Lindau, L. Porcar, M. Sepielli, M. Valli, Duncan J. McGillivray, Jill Trewhella, Elliot P. Gilbert, Tracey L. Hanley (Eds.), Proceedings of the 15th International Small-Angle Scattering Conference, 2012 ISBN 1 921.
[9] R. Coppola, M. Klimenkov, R. Lindau, B.R. Pauw, M. Valli, *Defect Distributions in Irradiated Nuclear Steels as Investigated with Complementary TEM and Small-Angle Neutron Scattering* Oral Presentation at the EMMM 2013 Conference, Kyoto, November 2013.
[10] R. Coppola, M. Klimenkov, A. Möslang, R. Lindau, M. Valli, Nucl. Mat. En. 9 (2016) 194–198.
[11] R. Coppola, M. Klimenkov, A. Möslang, R. Lindau, M. Rieth, M. Valli, Physica B (2017) *in print*.
[12] R. Coppola, Final Report EUROfusion Task MAT-5.5.5-T004-D001, Decembr 2017.
[13] A. Kumar, F.A. Garner, Rad. Eff. 82 (1984) 61–72.
[14] M. Klimenkov, E. Materna-Morris, U. Jäntsch, KIT Report 31.40.03, January 2013.
[15] G. Kostorz, X-ray and neutron scattering, in: R.W. Cahn, P. Haasen (Eds.), Physical Metallurgy, North Holland, 1983, pp. 793–853.
[16] M.T. Hutchings, C.G. Windsor, K. Sköld, D.L. Price (Eds.), Methods of Experimental Physics, vol 23-c, Neutron Scattering, Academic, 1987, pp. 405–482.
[17] E. Materna-Morris, M. Klimenkov, A. Möslang, Mat. Sc. For. 730-732 (2013) 877–882.
[18] M. Magnani, P. Puliti, M. Stefanon, Inst. Meth. A 217 (1988) 611–616.
[19] R. Coppola, R. Kampmann, M. Magnani, P. Staron, Acta Mat. 46 (1998) 5547–5566.
[20] R. Coppola, M. Klimiankou, R. Lindau, A. Möslang, M. Valli, J. Nucl. Mat. 329-333 (2004) 1057–1061.
[21] https://www.ill.eu/users/scientific-groups/large-scale-structures/grasp/.
[22] W. Qiang-Li, H. Kesternich, D. Schroeder, H. Schwahn, Ullmaier, Acta Met. Mat. 38 (1990) 2383–2392.
[23] G. Albertini, F. Carsughi, R. Coppola, W. Kesternich, F. Rustichelli, G. Mercurio, D. Schwahn, H. Ullmaier, J. Nuc. Mat. 191-194 (1992) 1327–1330.
[24] C. Dethloff, E. Gaganidze, J. Aktaa, Nucl. Mat. En. 9 (2016) 471–475.
[25] E. Gaganidze, J. Aktaa, Fus. Eng. Des. 88 (2013) 118–128.